Synthesizing Aza[n]helicenes to the Limit: Hydrogen-bond-assisted Solubility and Benzannulation Strategy

Yusuke Matsuo,† Masayuki Gon,† Kazuo Tanaka,† Shu Seki,† and Takayuki Tanaka*†

ABSTRACT: Synthetic challenges toward anomalous structures and electronic states often involve handling problems such as insolubility in common organic solvents and oxidative degradation under aerobic conditions. We designed benzo-annulated aza[n]helicenes, which benefit from both the suppressed elevation of HOMO energies and high solubility due to hydrogen-bonding with solvent molecules to overcome these challenges. This strategy enabled the synthesis of six new aza[n]helicenes (**[n]AH**s) of different lengths (n = 9–19) from acyclic precursors via one-shot oxidative fusion reactions. The structures of all the synthesized aza[n]helicenes were determined by X-ray diffraction (XRD) analysis, and their electrochemical potentials were measured by cyclic voltammetry. Among the synthesized aza[n]helicenes, **[17]AH** and **[19]AH** are the first heterohelicenes with a triple-layered helix. The noncovalent interaction (NCI) plots confirm the existence of an effective π-π interaction between the layers. The absorption and fluorescence spectra red-shifted as the helical lengths increased, without any distinct saturation points. The optical resolutions of *N*-butylated **[9]AH**, and **[11]AH** were accomplished and their circular dichroism (CD) and circularly polarized luminescence (CPL) were measured. Thus, the structural, (chir)optical, and electrochemical properties of the aza[n]helicenes were comprehensively analyzed.

INTRODUCTION

Helicene is a class of chiral π-conjugated molecules with a screw-shaped skeleton formed by *ortho*-fused benzene rings (*i.e.*, phenanthrene units) that has been actively studied.[1)] In addition to the chiroptical properties such as circular dichroism (CD) and circularly polarized luminescence (CPL),[2)] their physical properties as molecular springs[3)] and the CISS effect[4)] are cutting-edge functionalities based on the helical molecular scaffold. When focusing on the lengths of [n]carbohelicene, it is assumed that the overlap of the π-planes becomes more significant by forming a layered structure; double layered at n = 7 and triple layered at n = 13. In 2015, [16]carbohelicene (**A**) was synthesized by Murase and Fujita, and this is the longest [n]carbohelicene ever synthesized (Figure 1).[5)] The synthesis of longer helicenes has been desired simply as a synthetic challenge and various improved synthetic methods have been devised.[1c-g)] Helicenes comprising more than triple-layered structures are particularly difficult to synthesize, because of solubility issues, and because the middle-layered core is tightly compressed, making it difficult to release the strain. Recently, several longer helicene analogues that can release the strain by virtue of their structure have been developed. For example, expanded helicenes, in which phenanthrene units are partially replaced by anthracene units to increase the diameter of helicenes,[6)] and perylene bisimide-incorporated helicenes (helicene nanoribbons) have been synthesized.[7)] These "diameter-expanded" helicene analogues display interesting dynamic behavior and chiroptical properties. Tilly's group synthesized expanded [n]helicenes (**B**) with three different lengths (n = 15, 19, 23), and compared the racemization barriers and dissymmetry factors.[8)] By contrast, Hirose and Matsuda have reported "π-extended" [n]carbohelicenes (**C**) with three different lengths (n = 5, 7, 9), and compared their chiroptical properties, aromaticity, and ultrafast dynamics in the excited state.[9)] As another type of helicene analog, heterohelicenes, in which heteroatoms are embedded into the helicene backbones, have also attracted attention because of their excellent luminescence and redox properties.[10,11)] Generally, heterohelicenes are more electron-rich compared with carbohelicenes, thus their HOMO energy levels are continuously destabilized with the π-extension. Therefore, it is more difficult to synthesize longer heterohelicenes with full conjugation, whereas several heterohelicenes with a double-layered structure have been synthesized; one example is diazatrioxa-[13]helicene **D**.[12)] Furthermore, a triple-layered structure was accomplished with oxa[n]helicene **E** (n = 17, 19) albeit with disrupted π-conjugation.[13)] To qualitatively evaluate the electronic properties of helicenes, however, it is necessary to systematically synthesize fully conjugated heterohelicenes of different lengths, therefore, a synthetic strategy toward longer heterohelicene would be indispensable. Currently, few systematic synthetic methods are available for the synthesis of heterohelicenes.

We recently reported one-shot oxidative fusion reactions of *ortho*-phenylene-bridged oligopyrroles to afford various heterocirculenes and heterohelicenes.[14,15)] Notably, tetraaza[8]circulenes, with planar structures excluding any sterically encumbering substituents, are fairly soluble in THF and DMSO.[16)] This property arises from effective hydrogen-bonding interactions between the pyrrolic NH site and the H-bond accepting solvent molecule. Inspired by this molecular design principle, we report a synthetic challenge for longer azahelicenes with outer-pointing pyrrolic NH sites. By exploiting the one-shot oxidative fusion reactions of suitably designed indole-terminated acyclic oligopyrroles (*vide infra*), a series of benzannulated aza[n]helicenes were obtained. This structure is suitable for suppressing the

elevation of the HOMO energy levels by virtue of Clar's sextet rule.[17] In other words, the designed benzannulated aza[n]helicenes are an ideal platform to accomplish longer fully conjugated hetero[n]helicenes with respect to solubility and stability issues. Comprehensive characterizations by NMR, UV/Vis and fluorescence spectroscopy, electrochemistry, as well as CD and CPL spectra of the enantiomers revealed the π-conjugation along the helix and between the layers.

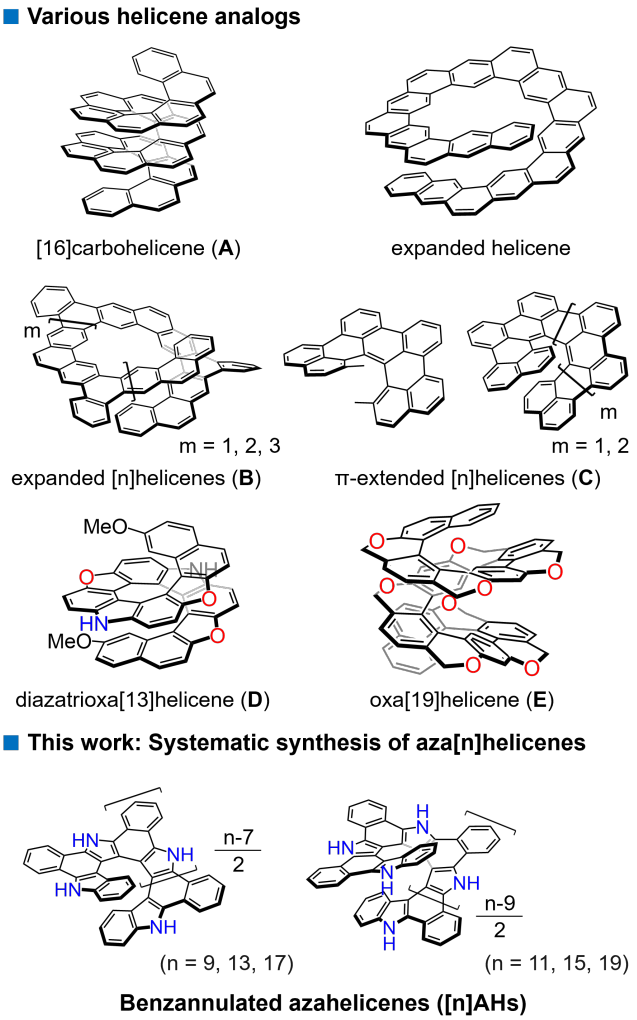

Figure 1. Various helicene analogs: longest [n]carbohelicene **A**, expanded helicenes **B**, extended helicenes **C**, heterohelicenes **D** and **E**. This work: benzannulated azahelicenes of different lengths (n = 9-19).

RESULTS AND DISCUSSION

Synthesis of aza[n]helicenes. In our previous study on the synthesis of dibenzoaza[7]helicenes, acyclic precursors like $\mathbf{6_7}$ were effectively utilized.[18] In this study, the extended analogs $\mathbf{6_n}$ and $\mathbf{8_n}$ were synthesized using Pd-catalyzed Suzuki–Miyaura cross-coupling reactions, followed by oxidation with [bis(trifluoroacetoxy)iodo]benzene (PIFA) to afford a series of benzannulated aza[n]helicenes (hereafter referred to as **[n]AH**) (n = 9, 11, 13, 15, 17, 19). In the case of aza[n]helicenes with n = 9, 13, 17, aryl bromides $\mathbf{3_m}$ were synthesized by Pd-catalyzed cross-coupling reactions of excess amounts of 1-bromo-2-iodobenzene or aryl dibromide $\mathbf{1_m}$ with α-borylated indole **2** (Scheme 1). Next, aryl boronic acid pinacol esters $\mathbf{4_m}$**-Bpin** were synthesized via cross-coupling reactions of $\mathbf{3_m}$ with α-borylated pyrrole and subsequent Ir-catalyzed borylation. Dipyrrole dibromide **5**[15] was coupled with a small excess of $\mathbf{4_m}$**-Bpin** in the presence of 5.0 mol% XPhos Pd G2 and excess potassium carbonate in THF/H_2O to afford the acyclic precursors $\mathbf{6_n}$. Finally, oxidative fusion reactions of the acyclic precursors with PIFA at low temperatures afforded the corresponding **[n]AH**s. For **[n]AH**s with n = 11, 15, 19, aryl bromides $\mathbf{3_m}$ were used as coupling partners. Tripyrrole diboronic acid pinacol ester **7**[15] was coupled with a small excess of the synthesized aryl bromides $\mathbf{3_m}$ in the presence of 5.0 mol% XPhos Pd G2 and an excess of potassium carbonate in THF/H_2O at room temperature to afford acyclic precursors $\mathbf{8_n}$, although the yields were moderate probably because of the competing protodeboronation reactions. Similarly, the oxidative fusion of acyclic precursors $\mathbf{8_n}$ by PIFA afforded **[n]AH**s. All six **[n]AH**s were purified using silica-gel column chromatography and recrystallization from THF/*n*-hexane in open air. All **[n]AH**s were characterized by ^{1}H- and ^{13}C-NMR, and HR-MS (See the Supporting Information, SI). ^{1}H-NMR spectra of the obtained **[n]AH**s were measured in DMSO-d_6 at room temperature with one drop of hydrazine monohydrate to prevent the generation of oxidized species.[19] For all **[n]AH**s, NMR spectra reflecting the C_2-symmetric structures were obtained. The terminal benzene protons (*indole-H*) shifted considerably upfield, indicating that these aromatic protons were located above other aromatic rings. Notably, upfield shifts in the signals in the aromatic region were observed as the helical length increased, probably because of the enhancement of anisotropic shielding by the π-electron of the stacked aromatic rings (Figure S3-45).

SCHEME 1. Synthesis of [n]AHs.

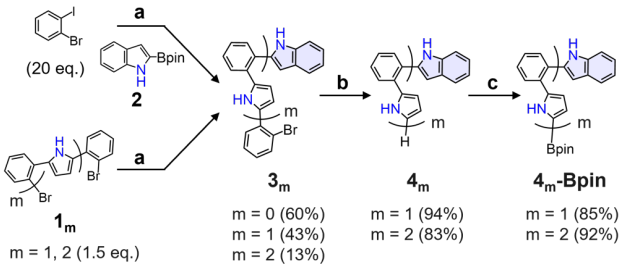

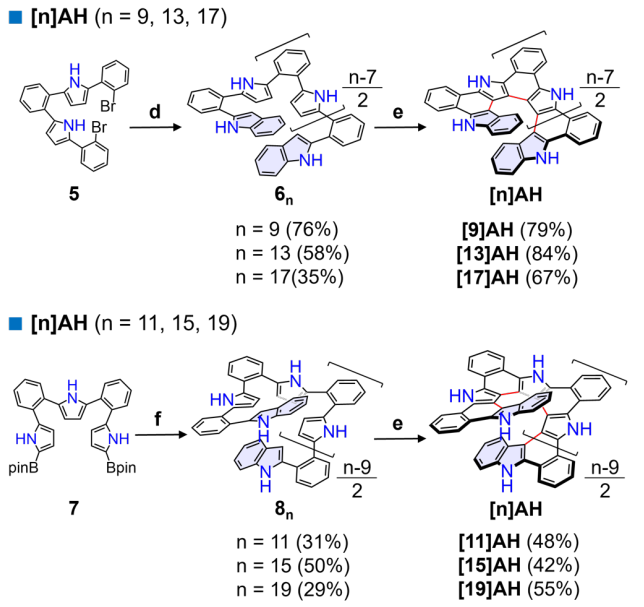

[a] $PdCl_2$(dppf) (5.0 mol%) or XPhos Pd G2 (5.0 mol%), K_3PO_4 (excess), 1,4-dioxane/H_2O or THF/H_2O, RT, 12 h or 24 h. [b] 2-(4,4,5,5-tetramethyl-1,3,2-dioxaborolan-2-yl)-1*H*-pyrrole (1.5 eq.), SPhos Pd G2 (m = 1; 2.5 mol%) or XPhos Pd G2 (m = 2; 5.0 mol%), K_3PO_4(excess), THF/H_2O, RT, 12 h. [c] $[Ir(cod)OMe]_2$ (1.0 mol%), DTBPY (3.0 mol%), B_2pin_2 (0.5 eq.), THF, 80 °C, 12 h. [d] **4_m-Bpin** (m = 0: 3.0 eq.; m = 1, 2: 2.5 eq.), XPhos Pd G2 (5.0 mol%), K_3PO_4 (excess), THF/H_2O, RT, 24 h. [e] 1) PIFA (n = 9: 6.0 eq.; n = 11: 8.0 eq.; n = 13, 15: 10 eq.; n = 17, 19: 12 eq.), CH_2Cl_2, –78 °C to RT, 3 h, 2) $NaBH_4$ (excess), MeOH, RT, 10 min. [f] **3_m** (m = 0: 2.2 eq.; m = 1: 2.6 eq.; m = 2: 2.1 eq.), XPhos Pd G2 (5.0 mol%), K_3PO_4 (excess), THF/H_2O, RT, 24 h.

X-ray crystal structures. Fortunately, single crystals suitable for X-ray diffraction (XRD) analysis were obtained by slow vapor diffusion of *n*-hexane into solutions of **[n]AH**s in THF, acetone, or 1,4-dioxane. The structures are shown in Figure 2A in which the solvent molecules coordinated to the NH moiety via hydrogen bonds are omitted. Because of the sophisticated molecular design, intermolecular interactions between **[n]AH**s were not observed in any of the structures, thereby contributing good solubility. Indeed, five and seven acetone molecules were included in the asymmetric units of **[13]AH** and **[15]AH**, respectively, (Figures S5-4, 5-5) whereas seven 1,4-dioxane molecules were included in the asymmetric unit of **[19]AH** (Figure S5-7). For **[9]AH**, the vertical distance (interplanar distance) between the centroid of terminal benzene ring A and the mean plain of the opposite terminal benzene ring I is 3.807 Å. As the typical distance of π-stacking is approximately 3.4 Å, interlayer interaction between the terminal benzene rings may be minimal, similarly to that of [7]carbohelicene (3.8–3.9 Å).[20] The interplanar angle between the stacked two benzene rings is approximately 40°, which also suggests that the interlayer π-π interaction is weak. By contrast, for **[11]AH**, the longest and shortest vertical distances are 3.567 Å and 3.202 Å, respectively, suggesting a distinct interlayer π-π interaction between the stacked aromatic rings. The interplanar angles are 16.3°, 11.6°, and 20.4°, being smaller than that of **[9]AH** in accordance with the effective interlayer π-π interactions. The crystal structures of **[13]AH** and **[15]AH** are also shown in Figure 2A. As the space group is $P3_2$ for the former and the lattice contains only one enantiomer, spontaneous chiral resolution took place for **[13]AH** upon crystallization. Chiral separation using HPLC apparatus is discussed later. In **[13]AH** and **[15]AH**, the shortest interplanar distances are less than 3.2 Å (3.199 Å and 3.176 Å), and the aromatic rings are very closely packed together, again confirming the existence of effective π-π interactions. The smallest interplanar angles are 3.3° and 1.4° for **[13]AH** and **[15]AH**, respectively. These values are even smaller than those of **[11]AH**. The crystal structures of **[17]AH** and **[19]AH** are the first examples of triple-layered fully conjugated heterohelicenes. In both **[17]AH** and **[19]AH**, the shortest interplanar distances are also less than 3.2 Å (3.170 Å and 3.185 Å, respectively), and the smallest interplanar angles are the smallest of those measured (1.2° and 0.8°). The interplanar angles at the ends are larger than those of the helicene central core due to the effect of electron repulsion and smaller steric constraints (**[19]AH**; θ_{AI} = 19.5°, θ_{FN} = 0.81°). However, at the center of the helicene core, the angles are almost 0°, because the central layers of **[17]AH** and **[19]AH** are located under large steric constraints from the top and bottom layers. After six types of crystal structures were obtained, their structural parameters of them (interplanar distance, interplanar angle, and dihedral angle) were compared with those of the obtained structures calculated at the B3LYP-D3(BJ)/def2-SVP level (Fig 2B).[21,22] For all the parameters, the trend of the experimentally determined values agreed with those obtained from the theoretical calculations, which reproduced the notable changes from **[9]AH** to **[11]AH**. This result reflects the weak intramolecular π-π interactions at the terminal aromatic ring of helicenes. A decrease in the interplanar distances or angles results in an increase in the dihedral angles, indicating that the intramolecular interactions become stronger and the aromatic rings become more densely stacked with helicene elongation, while the strain energies of the **[n]AH**s increase with helicene elongation. To estimate the inherent strain energy of **[n]AH**s, we attempted to adopt a homodesmotic reaction model.[23] Accordingly, the strain energy (ΔH) of **[n]AH**s increased continuously as the number '*n*' increased (Figure S7-12). These estimations are in accordance with several cases of expanded helicenes previously reported.[6d] Finally, the interlayer π-π interactions of **[n]AH**s between the two neighboring layers were visualized using the noncovalent interaction (NCI) plot analysis (Figures 2A and S7-11).[24] Dispersion interactions between the two stacked layers of **[n]AH**s are obvious (green surface shows intramolecular π-π interactions). In particular, intramolecular π-π interactions across three layers was confirmed for **[17]AH** and **[19]AH**.

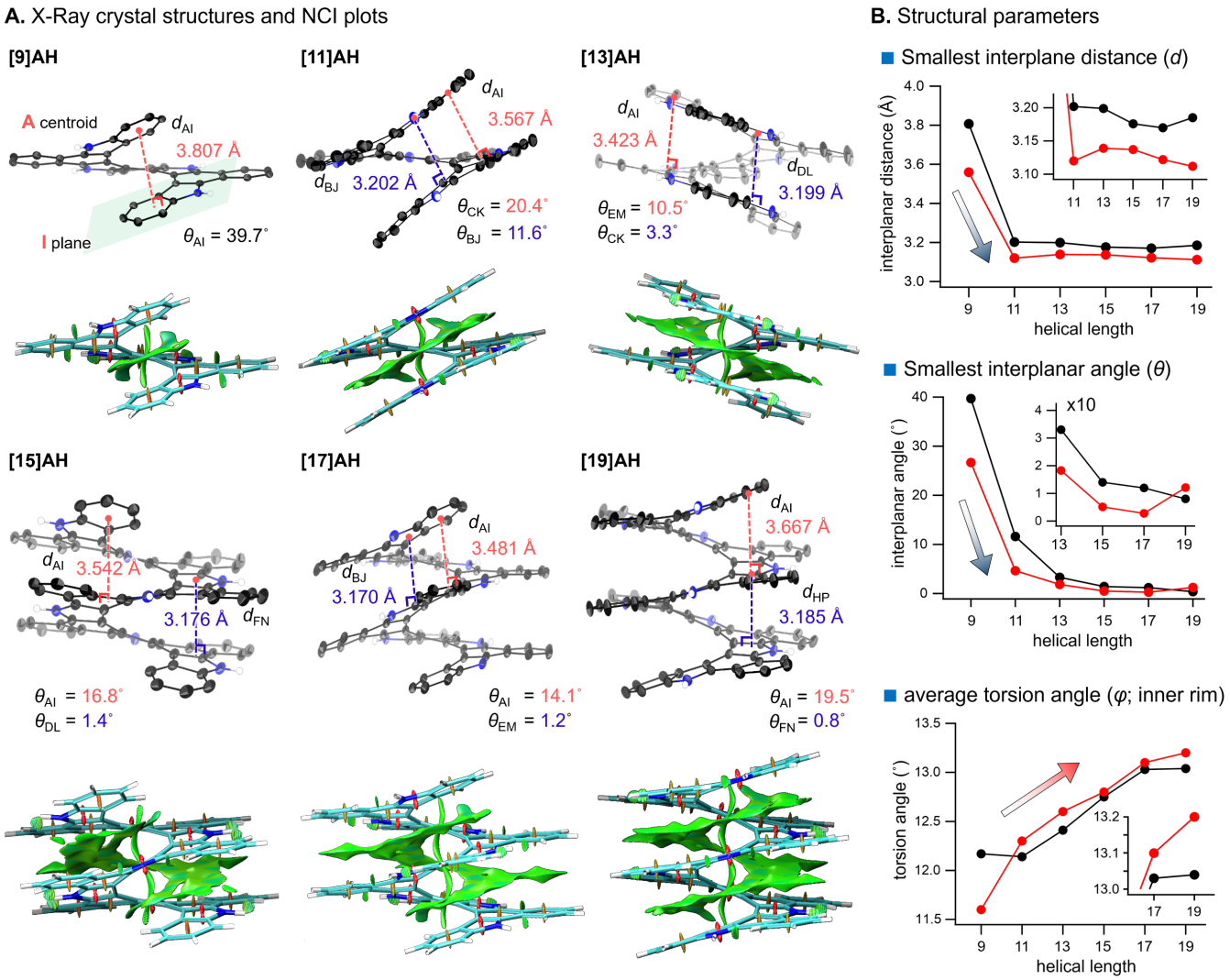

Figure 2. (A) X-Ray crystal structures (top) and NCI plots (bottom) of **[n]AH**s (isosurface: 0.50, Range: $-0.03 < \mathrm{sign}(\lambda_2)\rho < 0.03$). Thermal ellipsoids were scaled to 50% probability level. Solvent molecules and hydrogen atoms except for NHs have been omitted for clarity. (B) Comparison of structural parameters of **[n]AH**s. Crystal structure (black circle) and Optimized structure (B3LYP-D3(BJ)/def2-SVP level; red circle).

Electrochemical properties. The electrochemical properties of **[n]AH**s were measured using cyclic voltammetry (CV) and differential pulse voltammetry (DPV) in THF (Figure 3). All the **[n]AH**s exhibited reversible first oxidative waves, and the half-wave potential of **[9]AH** was recorded at +0.09 V against the ferrocene/ferrocenium ion couple. The longer **[n]AH**s exhibited negative potentials at –0.06 V for **[11]AH**, –0.16 V for **[13]AH**, –0.26 V for **[15]AH**, –0.38 V for **[17]AH**, and –0.48 V for **[19]AH**. The negative shift in the first oxidation potentials can be attributed to an increase in the number of electron-rich pyrrole units in the helicene core. In particular, **[19]AH** was confirmed to be very easily oxidized. Nevertheless, the as-synthesized **[19]AH** was purified using flash chromatography on silica at room temperature and recrystallized from THF/*n*-hexane, allowing the growth of single crystals under ambient conditions (*vide supra*). Molecular orbital calculations were performed for the optimized structures of **[n]AH** in the ground state (Figure 4). The HOMO energy level gradually increased as the helical length increased. By contrast, the LUMO energy level was not markedly affected by the elongation, resulting in a gradual decrease in the HOMO-LUMO gaps. To gain further insight into the structure-property relationship in these benzannulated azahelicenes, the corresponding aza[n]helicenes without benzannulated structures (*i.e.*, **[n]AH'**) were also calculated (Figure S7-8).[25] The HOMO energy levels of **[n]AH'**s are generally higher than those of **[n]AH**s by 0.11–0.37 eV (*e.g.* –4.45 V for **[19]AH** vs –4.18 V for **[19]AH'**). Therefore, as a proof-of-concept, the benzannulated molecular design principle contributes to the stabilization of the longer aza[n]helicenes.

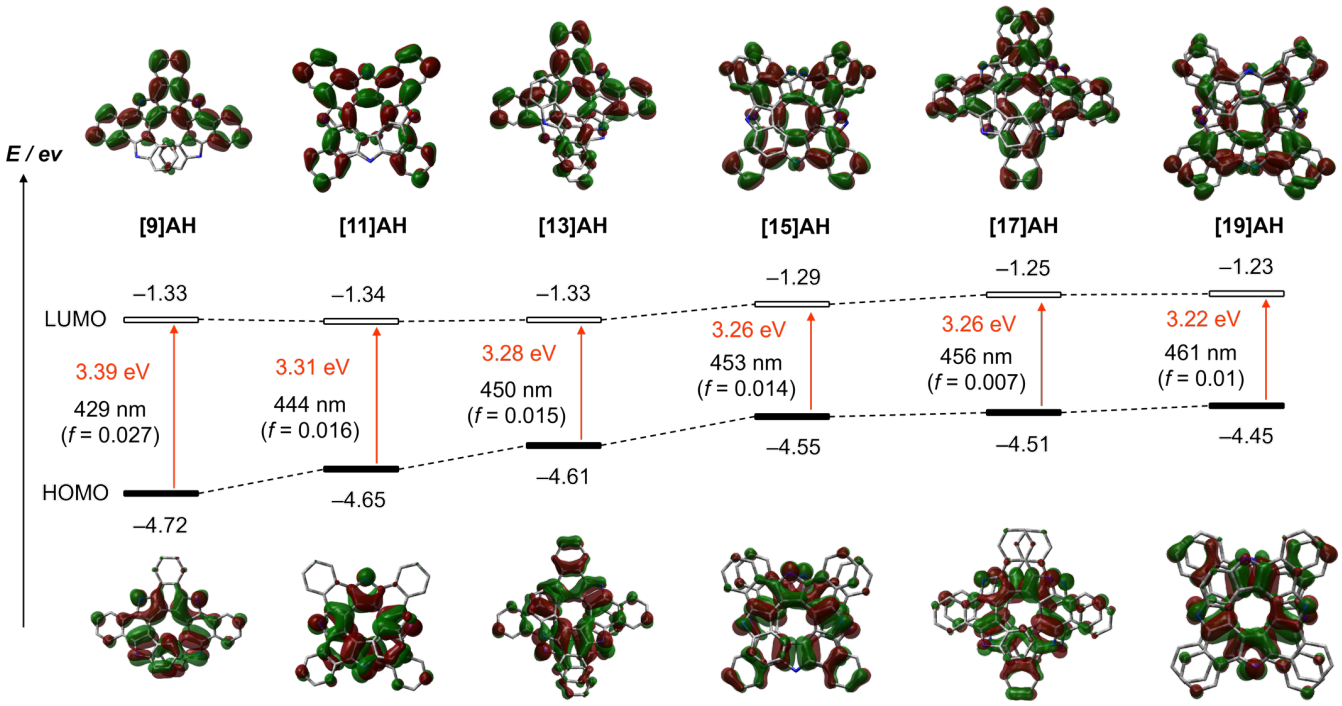

Figure 4. Kohn–Sham MO representation and energy diagrams of **[n]AH**s calculated at the (TD-)B3LYP-D3(BJ)/def2-SVP level.

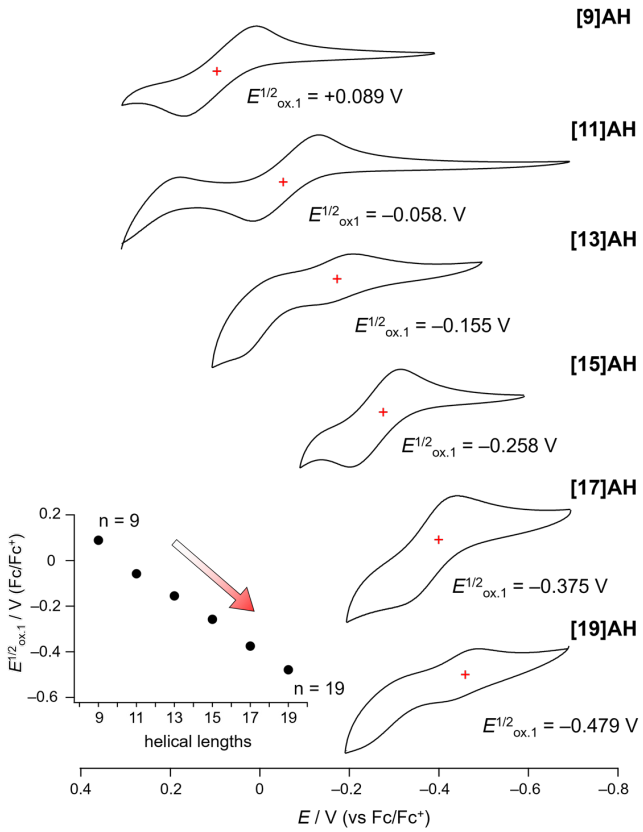

Figure 3. Cyclic voltammograms of **[n]AH**s. (solvent: THF, electrolyte: 0.1 M *n*-Bu_4NPF_6, working electrode: Pt, counter electrode: Pt, reference electrode: $Ag/AgNO_3$, scan rate: 0.05 V/s.)

Aromaticity. To evaluate the aromaticity of **[n]AH**s, the NICS(0) value at the center of each rings was calculated using the GIAO method at the B3LYP/6-311G(d,p) level based on the optimized structures.[26] The NICS(0) values of **[9]AH** and **[11]AH** are in the range from –6.6 to –11.6 ppm and from –6.3 to –12.3 ppm, respectively (Figure 5A). Rings 3 and 5 were relatively shielded whereas the local aromaticity in the pyrrole units (Rings 2, 4, (6)) and the terminal benzene moiety (ring 1) were dominant. The HOMA values are consistent with the local aromaticity of these rings.[27] Notably, the benzo segments (rings 6 and 7 for **[9]AH** and rings 7 and 8 for **[11]AH**) exhibit relatively deshielded features compared with the neighboring six-membered ring. The anisotropy of the induced current density (ACID) calculations[28] revealed the localized aromatic ring-current flows of the pyrrole and the annulated benzene rings in **[9]AH** and **[11]AH** as the dominant contributions (Figure 4B). These results represented Clar's sextet rule as shown in Figure 4C. Such local aromaticity suppresses the increase in the HOMO energy levels to the extent that the isolation of these molecules without any kinetically stabilizing substituents is allowed under air. The same calculations were performed for longer **[n]AH** and the same trend in their aromaticity was observed (Figures S7-9, S7-10).

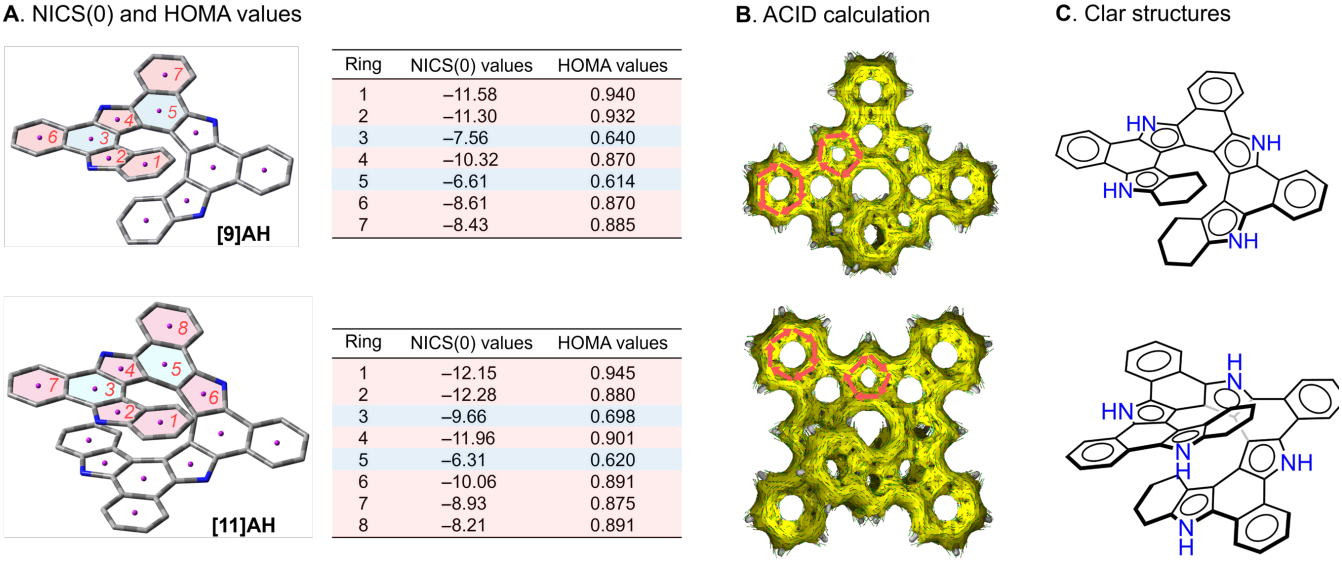

Ring	NICS(0) values	HOMA values
1	–11.58	0.940
2	–11.30	0.932
3	–7.56	0.640
4	–10.32	0.870
5	–6.61	0.614
6	–8.61	0.870
7	–8.43	0.885

Ring	NICS(0) values	HOMA values
1	–12.15	0.945
2	–12.28	0.880
3	–9.66	0.698
4	–11.96	0.901
5	–6.31	0.620
6	–10.06	0.891
7	–8.93	0.875
8	–8.21	0.891

Figure 5. (A) Calculated NICS(0) values at the selected points and HOMA values. (B) ACID isosurfaces of **[9]AH** (top) and **[11]AH** (bottom). For ACID calculations, the external magnetic field was applied in the direction from the back of the paper to the surface and the isosurface value was set at 0.05. (C) Clar structures of **[9]AH** and **[11]AH**.

(Chir)optical properties. The UV/vis absorption and fluorescence spectra of a series of aza[n]helicenes were measured in THF at room temperature (Figures 6A and 6B). The edges of the absorption spectra are red-shifted, and the molar extinction coefficient (ε) increases with helicene π-extension. In particular, the absorption spectral edge of the longest **[19]AH** reaches approximately 500 nm, suggesting that the effective conjugation length (ECL) in this system was not saturated.[29] This result was supported by the HOMO-LUMO energy gaps obtained from theoretical calculations (Figure S7-7). All the aza[n]helicenes exhibited blue-to-yellow luminescence with some vibrational bands. The edges of the fluorescence spectra also show gradual red-shifts along with the helicene π-extension. The absolute fluorescence quantum yields (Φ_F) tended to decrease with increasing helical length (*e.g.* Φ_F = 0.21 for **[9]AH** and Φ_F = 0.08 for **[19]AH**) (Figure 6C). However, even **[19]AH** exhibits distinct blue-green fluorescence with Φ_F = 0.08 as a characteristic feature of heterohelicenes. By contrast, **[17]AH** exhibits a high fluorescence quantum yield with Φ_F = 0.18, which may be attributed to its rigid structure and suppressed nonradiative deactivation as a result of the large steric constraints caused by the triple-layered structure.

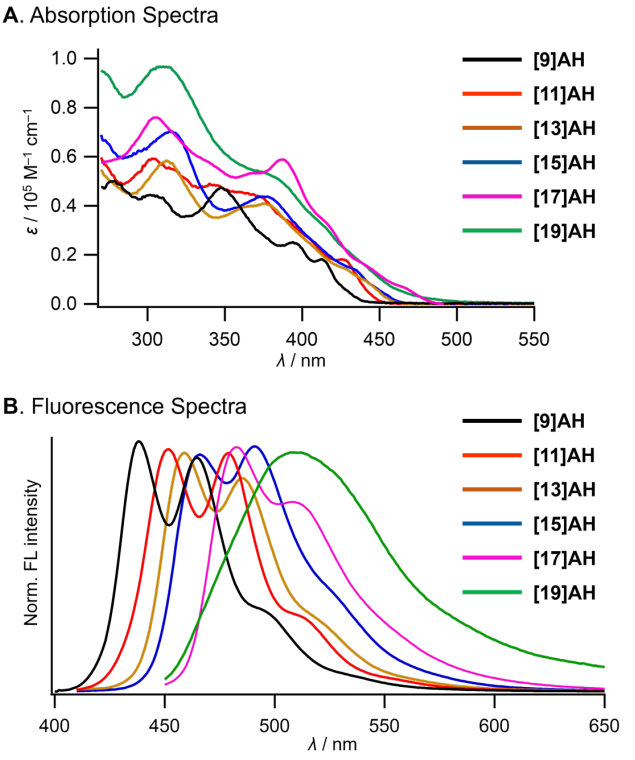

C. Summery of optical properties

[n]AH	[9]AH	[11]AH	[13]AH	[15]AH	[17]AH	[19]AH
λ_{em} / nm	423	452	459	466	483	508
Φ_F	0.21	0.17	0.11	0.09	0.18	0.08

Figure 6. (A) Electronic absorption and (B) fluorescence spectra of **[n]AH**s in THF at room temperature (FL: λ_{ex} = 380 or 440 nm). (C) Summary of peak wavelength and absolute fluorescence quantum yield (bottom).

The chiral resolution was examined using HPLC equipped with a chiral stationary phase to investigate the chiroptical properties of **[n]AH**s. Despite the adoption of numerous conditions, the enantiomers could not be separated, except for **[9]AH**. The inability to separate the enantiomers may be partly ascribed to the limitations of the solvent, which was eluted as a gradient. Thus, we focused on *N*-alkylation of **[n]AH**s to improve their solubility in various organic solvents. Recently, we reported that *N*-alkylation of aza[8]circulenes improves their solubilities and stabilities owing to the lowered HOMO energy levels.[30] Thus, we performed *N*-alkylation of **[n]AH**s with an excess of 1-iodobutane in the presence of ^{t}BuOK in DMSO at room temperature (Scheme 2). Completely *N*-butylated aza[n]helicenes (n = 9, 11, 13), namely **[9]AH-Bu$_4$**, **[11]AH-Bu$_5$**, and **[13]AH-Bu$_6$**, were obtained in moderate yields. The ^{1}H NMR spectra of the three **[n]AH-Bu** in CD_2Cl_2 showed no peaks attributable to NH protons, and XRD measurements confirmed the presence of *N*-butyl groups on all pyrrole moieties (Figures S5-14, S5-15, S5-16). However, for **[15]AH** and **[17]AH**, incompletely *N*-alkylated derivatives, **[15]AH-Bu$_6$** and **[17]AH-Bu$_6$**, were obtained (Scheme 3). The ^{1}H NMR spectra of **[15]AH-Bu$_6$** and **[17]AH-Bu$_6$** displayed broad peaks at 8.49 and 7.91 ppm, respectively, which were assigned to NH (Figure S3-46). The XRD measurements also confirmed that the pyrrole units in the azahelicene core remained undreacted in the middle layer (Figures S5-17, S5-18). Presumably, for **[15]AH** and **[17]AH**, the central NH moieties are less reactive owing to the steric hindrance caused by the upper and lower layers. Unfortunately, **[19]AH** was not cleanly derivatized under the same conditions, which resulted in the formation of a complex mixture, probably because of its highly electron-rich core. With these *N*-butyl aza[n]helicenes, enantiomeric separation could be accomplished by using chiral stationary phases with **[9]AH-Bu$_4$** and **[11]AH-Bu$_5$** (Fig. S9-1). The CD spectra of both the first and second eluents were measured to display mirror-imaged spectra (Figure 7A). The spectra showing a positive-to-negative Cotton effect around 350 nm were those of the first eluted solutions in all cases, which was assigned as (*M*)-enantiomers, as determined by TD-DFT calculations (Figure S9-4). The intensities of the main bands of the molar circular dichroism ($\Delta\varepsilon$) with the maxima located at 328 nm and the dissymmetry factors (g_{CD}) measured for **[9]AH-Bu$_4$** were: $|\Delta\varepsilon|$ = 186 M^{-1} cm^{-1}, $|g_{CD}| = |\Delta\varepsilon/\varepsilon| = 5.6 \times 10^{-3}$. For **[11]AH-Bu$_5$**, $|\Delta\varepsilon|$ = 166 M^{-1} cm^{-1} and $|g_{CD}| = 4.2 \times 10^{-3}$ at 326 nm. Furthermore, the *N*-butylated aza[n]helicenes exhibited mirror-imaged CPL spectra in THF (Figure 7B). The $|g_{CPL}|$ value of 10^{-3} order was recorded (**[9]AH-Bu$_4$**: 445 nm: $|g_{CPL}| = 4.5 \times 10^{-3}$; **[11]AH-Bu$_5$**: 479 nm: $|g_{CPL}| = 4.2 \times 10^{-3}$). Finally, we examined the dissymmetry factors of the azahelicenes using TD-DFT calculations. A clear trend of improved chiroptical response as a function of the helicene length was revealed (Figure S9-7). The behavior of **[n]AH** in racemization is clarified using theoretical calculations at the B3LYP-D3(BJ)/def2-SVP level. The results showed that the most stable structures had C_2 symmetry and the transition states had C_s symmetry. As indicated in our previous study,[18] the inversion barrier at 298 K was relatively smaller (+24.3 kcal/mol) for **[7]AH**, which has no overlapping aromatic rings in the molecule, while the value is clearly larger (+45.8 kcal/mol) for **[9]AH** which comprises overlapping aromatic rings (Figure S9-5). The value increases slightly with helicene elongation (*e.g.*, +51.1 kcal/mol for **[11]AH**) (Figure S9-6).[31] Consistently, none of the aza[n]helicenes enantiomerically purified in this study showed racemization at room temperature.

SCHEME 2. Synthesis of *N*-Butyl Aza[n]helicenes (n = 9, 11, 13).

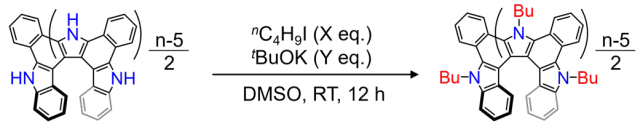

[n]AH (n = 9, 11, 13) → **[n]AH-Bu$_m$** [m = (n–1)/2]

[n]AH	*n*-C$_4$H$_9$I	^{t}BuOK	yield
[9]AH	400 eq.	40 eq.	82% (95% per unit)
[11]AH	500 eq.	50 eq.	58% (90% per unit)
[13]AH	600 eq.	60 eq.	59% (92% per unit)

SCHEME 3. Synthesis of *N*-Butyl Aza[n]helicenes (n = 15, 17).

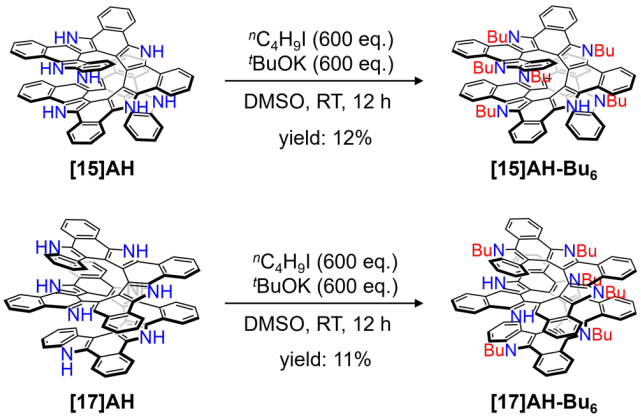

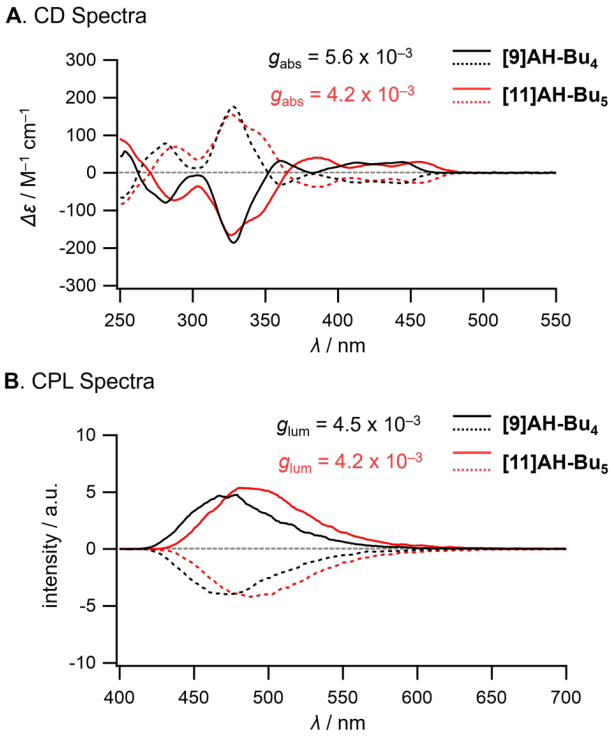

https://doi.org/10.26434/chemrxiv-2023-4z7z6 **ORCID:** https://orcid.org/0000-0001-8018-7984

Figure 7. (A) CD and (B) CPL spectra of **[9]AH-Bu$_4$** (black) and **[11]AH-Bu$_5$** (red) in THF at room temperature (CPL: λ_{ex} = 330 nm). (solid lines and dashed lines indicate either (*P*) or (*M*)).

CONCLUSIONS

In conclusion, six new aza[n]helicenes (**[n]AH**) of different lengths (n = 9, 11, 13, 15, 17, 19) were successfully synthesized from acyclic precursors via one-shot oxidative fusion reactions with PIFA. The structures of all synthesized azahelicenes were determined using XRD analysis. **[17]AH** and **[19]AH** are the first heterohelicenes with a triple-layered helix. The structural parameters of the helicenes (*i.e.*, interplanar distance, interplanar angle, and torsion angle) were compared experimentally and theoretically. The intramolecular interactions became stronger and the aromatic rings became more densely stacked with the elongation of the helical structure. The NCI plots confirmed the existence of an effective π-π interaction between the layers. Electrochemical potentials were measured using CV, and the first oxidation potential shifted to the negative side in response to helicene elongation. The absorption and fluorescence spectra red-shifted as the helical lengths increased, without any distinct saturation points. The optical resolutions of *N*-butylated **[9]AH** and **[11]AH** were accomplished, and their CD and CPL spectra were measured. The molecular design of the azahelicenes synthesized in this study solves the stability and solubility problems encountered thus far, and may provide an ideal platform for the synthesis of longer heterohelicenes.

ASSOCIATED CONTENT

Supporting Information

The Supporting Information is available free of charge on the ACS Publications website.

Synthesis procedures, characterization data, details of the photophysical measurements, and NMR spectra of all new compounds (PDF)

X-ray structure of **6$_9$** (CIF)
X-ray structure of **[9]AH** (CIF)
X-ray structure of [**11]AH** (CIF)
X-ray structure of **[13]AH** (CIF)
X-ray structure of **[15]AH** (CIF)
X-ray structure of **[17]AH** (CIF)
X-ray structure of **[19]AH** (CIF)
X-ray structure of **[9]AH-Bu$_4$** (CIF)
X-ray structure of **[11]AH-Bu$_5$** (CIF)
X-ray structure of **[13]AH-Bu$_6$** (CIF)
X-ray structure of **[15]AH-Bu$_6$** (CIF)
X-ray structure of **[17]AH-Bu$_6$** (CIF)

Accession Codes

CCDC 2307724–2307734, 2307776 contain the supplementary crystallographic data for this paper. These data can be obtained free of charge via www.ccdc.cam.ac.uk/data_request/cif,or by emailing data_request@ccdc.cam.ac.uk, or by contacting The Cambridge Crystallographic Data Centre, 12 Union Road, Cambridge CB2 1EZ, UK; fax: +441223 336033

AUTHOR INFORMATION

Corresponding Author

* Takayuki Tanaka - *Department of Molecular Engineering, Graduate School of Engineering, Kyoto University, Nishikyo-ku, Kyoto 615-8510 (Japan)*
https://orcid.org/0000-0001-8018-7984
E-mail: tanaka@moleng.kyoto-u.ac.jp

Yusuke Matsuo - *Department of Chemistry, Graduate School of Science, Kyoto University, Sakyo-ku, Kyoto 606-8502 (Japan)*
E-mail: matsuo@shuyu.kuchem.kyoto-u.ac.jp

Masayuki Gon - *Department of Polymer Chemistry, Graduate School of Engineering, Kyoto University, Nishikyo-ku, Kyoto 615-8510 (Japan)*
E-mail: gon@poly.synchem.kyoto-u.ac.jp

Kazuo Tanaka - *Department of Polymer Chemistry, Graduate School of Engineering, Kyoto University, Nishikyo-ku, Kyoto 615-8510 (Japan)*
E-mail: tanaka@poly.synchem.kyoto-u.ac.jp

Shu Seki- *Department of Molecular Engineering, Graduate School of Engineering, Kyoto University, Nishikyo-ku, Kyoto 615-8510 (Japan)*
E-mail: seki@moleng.kyoto-u.ac.jp

Takayuki Tanaka - *Department of Molecular Engineering, Graduate School of Engineering, Kyoto University, Nishikyo-ku, Kyoto 615-8510 (Japan)*
E-mail: tanaka@moleng.kyoto-u.ac.jp

Notes

The authors declare no competing financial interests.

ACKNOWLEDGMENT

This work was supported by JSPS KAKENHI Grant Numbers (21H05480, 22H00314 and 23K17942) and CREST, Japan Science and Technology Agency (JST). T.T. gratefully acknowledges the Asahi Glass Foundation and ISHIZUE 2023 of Kyoto University. Y. M. acknowledges the JSPS fellowships for young scientists.

REFERENCES

[1] a) Martin, R. H. The Helicenes. *Angew. Chem. Int. Ed. Engl.* **1974**, *13*, 649; b) Grimme, S.; Harren, J.; Sobanski, A.; Vögtle, F. Structure/Chiroptics Relationships of Planar Chiral and Helical Molecules. *Eur. J. Org. Chem.* **1998**, 1491; c) Shen, Y.; Chen, C.-Y. Helicenes: Synthesis and Applications. *Chem. Rev.* **2012**, *112*, 1463; d) Gingras, M. One hundred years of helicene chemistry. Part 1: non-stereoselective syntheses of carbohelicenes. *Chem. Soc. Rev.* **2013**, *42*, 968; e) Gingras, M.; Félix, G.; Peresutti, R. One hundred years of helicene chemistry. Part 2: stereoselective syntheses and chiral separations of carbohelicenes. *Chem. Soc. Rev.* **2013**, *42*, 1007; f) Gingras, M. One hundred years of helicene chemistry. Part 3: applications and properties of carbohelicenes. *Chem. Soc. Rev.* **2013**, *42*, 1051; g) Ravat, P. Carbo[n]helicenes Restricted to Enantiomerize: An Insight into the Design Process of Configurationally Stable Functional Chiral PAHs. *Chem. Eur. J.* **2021**, *27*, 3957.

[2] a) Zhao, W.-L.; Li, M.; Lu, H.-Y.; Chen, C.-F. Advances in helicene derivatives with circularly polarized luminescence. *Chem. Commun.* **2019**, *55*, 13793; b) Mori, T. Chiroptical Properties of Symmetric Double, Triple, and Multiple Helicenes. *Chem. Rev.* **2021**, *121*, 2373; c) Cei, M.; Bari, L. D.; Zinna, F. Circularly polarized luminescence of helicenes: A data-informed insight. *Chirality* **2023**, *35*, 192.

[3] a) Guo, Y.-D.; Yan, X.-H.; Xiao, Y.; Liu, C.-S. U-shaped relationship

between current and pitch in helicene molecules. *Sci*. *Rep*. **2015**, *5*, 16731; b) Karak, P.; Choudhury, J. Conformationally flexible heterohelicenes as stimuli-controlled soft molecular springs. *Chem*. *Sci*. **2022**, *13*, 11163.

[4] a) Kiran, V.; Mathew, S. P.; Cohen, S. R.; Delgado, I. H.; Lacour, J.; Naaman, R. Helicenes—A New Class of Organic Spin Filter. *Adv*. *Mater*. **2016**, *28*, 1957; b) Kettner, M.; Maslyuk, V. V.; Nürenberg, D.; Seibel, J.; Gutierrez, R.; Cuniberti, G.; Ernst, K.-H.; Zacharias, H. Chirality-Dependent Electron Spin Filtering by Molecular Monolayers of Helicenes. *J*. *Phys*. *Chem*. *Lett*. **2018**, *9*, 2025; c) Rodríguez, R.; Naranjo, C.; Kumar, A.; Matozzo, P.; Das, T. K.; Zhu, Q.; Vanthuyne, N.; Gómez, R.; Naaman, R.; Sánchez, L.; Crassous, J. Mutual Monomer Orientation To Bias the Supramolecular Polymerization of [6]Helicenes and the Resulting Circularly Polarized Light and Spin Filtering Properties. *J*. *Am*. *Chem*. *Soc*., **2022**, *144*, 7709; d) Giaconi, N.; Poggini, L.; Lupi, M.; Briganti, M.; Kumar, A.; Das, T. K.; Sorrentino, A. L.; Viglianisi, C.; Menichetti, S.; Naaman, R.; Sessoli, R.; Mannini, M. Efficient Spin-Selective Electron Transport at Low Voltages of Thia-Bridged Triarylamine Hetero[4]helicenes Chemisorbed Monolayer. *ACS Nano* **2023**, *17*, 15189.

[5] Mori, K.; Murase, T.; Fujita, M. *Angew. Chem. Int. Ed.* **2015**, *54*, 6847.

[6] a) Kiel, G. R.; Patel, S. C.; Smith, P. W.; Levine, D. S.; Tilley, T. D. Expanded Helicenes: A General Synthetic Strategy and Remarkable Supramolecular and Solid-State Behavior. *J*. *Am*. *Chem*. *Soc*. **2017**, *139*, 18456; b) Fujise, K.; Tsurumaki, E.; Wakamatsu, K.; Toyota, S. Construction of Helical Structures with Multiple Fused Anthracenes: Structures and Properties of Long Expanded Helicenes. *Chem*. *Eur*. *J*. **2021**, *27*, 4548; c) Nakakuki, Y.; Hirose, T.; Matsuda, K. Synthesis of a Helical Analogue of Kekulene: A Flexible π-Expanded Helicene with Large Helical Diameter Acting as a Soft Molecular Spring. *J*. *Am*. *Chem*. *Soc*. **2018**, *140*, 15461; d) Toya, M.; Omine, T.; Ishiwari, F.; Saeki, A.; Ito, H.; Itami, K. Expanded [2,1][n]Carbohelicenes with 15- and 17-Benzene Rings. *J*. *Am*. *Chem*. *Soc*. **2023**, *145*, 11553.

[7] a) Schuster, N. J.; Sánchez, R. H.; Bukharina, D.; Kotov, N. A.; Berova, N.; Ng, F.; Steigerwald, M. L.; Nuckolls, C. A Helicene Nanoribbon with Greatly Amplified Chirality. *J*. *Am*. *Chem*. *Soc*. **2018**, *140*, 6235; b) Xiao, X.; Pedersen, S. K.; Aranda, D.; Yang, J.; Wiscons, R. A.; Pittelkow, M.; Steigerwald, M. L.; Santoro, F.; Schuster, N. J.; Nuckolls, C. Chirality Amplified: Long, Discrete Helicene Nanoribbons. *J*. *Am*. *Chem*. *Soc*. **2021**, *143*, 983; c) Xiao, X.; Cheng, Q.; Bao, S. T.; Jin, Z.; Sun, S.; Jiang, H.; Steigerwald, M. L.; Nuckolls, C. Single-Handed Helicene Nanoribbons via Transfer of Chiral Information. *J*. *Am*. *Chem*. *Soc*. **2022**, *144*, 20214.

[8] Kiel, G. R.; Bergman, H. M.; Samkian, A. E.; Schuster, N. J.; Handford, R. C.; Rothenberger, A. J.; Gomez-Bombarelli, R.; Nuckolls, C.; Tilley, T. D. Expanded [23]-Helicene with Exceptional Chiroptical Properties via an Iterative Ring-Fusion Strategy. *J*. *Am*. *Chem*. *Soc*. **2022**, *144*, 23421.

[9] a) Nakakuki, Y.; Hirose, T.; Sotome, H.; Miyasaka, H.; Matsuda, K. Hexa-*peri*-hexabenzo[7]helicene: Homogeneously π-Extended Helicene as a Primary Substructure of Helically Twisted Chiral Graphenes. *J*. *Am*. *Chem*. *Soc*. **2018**, *140*, 4317; b) Nakakuki, Y.; Hirose, T.; Sotome, H.; Gao, M.; Shimizu, D.; Li, R.; Hasegawa, J.; Miyasaka, H.; Matsuda, K. Doubly linked chiral phenanthrene oligomers for homogeneously π-extended helicenes with large effective conjugation length. *Nat. Commun*. **2022**, *13*, 1475.

[10] a) Wynberg, H.; Groen, M. B. Synthesis, resolution, and optical rotatory dispersion of a hexa- and a heptaheterohelicene. *J. Am. Chem. Soc.* **1968**, *90*, 5339; b) Wynberg, H. Some Observations on the Chemical, Photo-chemical, and Spectral Properties of Thiophenes. *Acc. Chem. Res.* **1971**, *4*, 65; c) Stary, I.; Stara, I. G.; Alexandrova, Z.; Sehnal, P.; Teply, F.;Saman, D.; Rulisek, L. Helicity Control in The Synthesis of Helicenesand Related Compounds. *Pure Appl. Chem.* **2006**, *78*, 495; d) Collins, S. K.; Vachon, M. P. Unlocking the Potential of Thiaheterohelicenes: Chemical Synthesis as the Key. *Org. Biomol. Chem.* **2006**, *4*, 2518-2524; e) Dhbaibi, K.; Favereau, L.; Crassous, J. Enantioenriched Helicenes and Helicenoids Containing Main-GroupElements (B, Si, N, P). *Chem. Rev.* **2019**, *119*, 8846; f) Jakubec, M.; Storch, J. Recent Advances in Functionalizations of Helicene Backbone. *J. Org. Chem.* **2020**, *85*, 13415; g) Stará, I. G.; Starý, I. Helically Chiral Aromatics: The Synthesis of Helicenes by [2+2+2] Cycloisomerization of π-Electron Systems. *Acc. Chem*. *Res*. **2020**, *53*, 144.

[11] Selected examples; a) Sundar, M. S. Bedekar, A. V. Synthesis and Study of 7,12,17-Trioxa[11]helicene. *Org*. *Lett*. **2015**, *17*, 5808; b) Otani, T.; Tsuyuki, A.; Iwachi, T.; Someya, S.; Tateno, K.; Kawai, H.; Saito, T.; Kanyiva, K. S.; Shibata, T. Facile Two-Step Synthesis of 1,10-Phenanthroline-Derived Polyaza[7]helicenes with High Fluorescence and CPL Efficiency. *Angew*. *Chem*. *Int*. *Ed*. **2017**, *56*, 3906; c) Chen, F.; Tanaka, T.; Hong, Y. S.; Mori, T.; Kim, D.; Osuka, A. Closed Pentaaza[9]helicene and Hexathia[9]/[5]helicene: Oxidative Fusion Reactions of *ortho*-Phenylene-Bridged Cyclic Hexapyrroles and Hexathiophenes. *Angew. Chem. Int. Ed.* **2017**, *56*, 1468; d) Yanagi, T.; Tanaka, T.; Yorimitsu, H. Asymmetric systematic synthesis, structures, and (chir)optical properties of a series of dihetero[8]helicenes. *Chem. Sci.* **2021**, *12*, 2784; e) Oda, S.; Kawakami, B.; Yamasaki, Y.; Matsumoto, R.; Yoshioka, M.; Fukushima, D.; Nakatsuka, S.; Hatakeyama, T. One-Shot Synthesis of Expanded Heterohelicene Exhibiting Narrowband Thermally Activated Delayed Fluorescence. *J*. *Am*. *Chem*. *Soc*. **2022**, *144*, 106; f) Volland, D.; Niedens, J.; Geppert, P. T.; Wildervanck, M. J.; Full, F.; Nowak-Król, A. Synthesis of a Blue-Emissive Azaborathia[9]helicene by Silicon-Boron Exchange from Unusual Atropisomeric Teraryls. *Angew*. *Chem*. *Int*. *Ed*. **2023**, *62*, e202304291; g) Khalid, M. I.; Salem, M. S. H.; Sako, M.; Kondo, M.; Sasai, H.; Takizawa, S. Electrochemical synthesis of heterodehydro[7]helicenes. *Commun. Chem.* **2022**, *5*, 166.

[12] a) Pedersen, S. K.; Eriksen, K.; Pittelkow, M. Symmetric, Unsymmetrical, and Asymmetric [7]-, [10]-, and [13]Helicenes. *Angew*. *Chem*. *Int*. *Ed*. **2019**, *58*, 18419; b) Warthegau, S. S.; Hillers-Bendtsen, A. E.; Pedersen, S. K.; Rindom, C.; Bræstrup, C.; Jensen, J. S.; Hammerich, O.; Thomsen, M. S.; Kamounah, F. S.; Norman, P.; Mikkelsen, K. V.; Brock-Nannestad, T.; Pittelkow, M. Heterocyclic [9]Helicenes Exhibiting Bright Circularly Polarized Luminescence. *Chem. Eur. J.* **2023**, *29*, e202301815.

[13] Nejedlý, J.; Šámal, M.; Rybáček, J.; Tobrmanová, M.; Szydlo, F.; Coudret, C.; Neumeier, M.; Vacek, J.; Chocholoušová, J. V.; Buděšínský, M.; Šaman, D.; Bednárová, L.; Sieger, L.; Stará, I. G.; Starý, I. Synthesis of Long Oxahelicenes by Polycyclization in a Flow Reactor. *Angew*. *Chem*. *Int*. *Ed*. **2017**, *56*, 5839.

[14] Tanaka, T. Synthesis of Novel Heteronanographenes via Fold-in Approach. *Bull. Chem. Soc. Jpn.* **2022**, *95*, 602.

[15] Matsuo, Y.; Kise, K.; Morimoto, Y.; Osuka, A.; Tanaka, T. Fold-in Synthesis of a Pentabenzopentaaza[10]circulene. *Angew*. *Chem*. *Int*. *Ed*. **2022**, *61*, e202116789.

[16] a) Chen, F.; Hong, Y. S.; Shimizu, S.; Kim, D.; Tanaka, T.; A. Osuka, A. Synthesis of a Tetrabenzotetraaza[8]circulene by a "Fold-In" Oxidative Fusion Reaction. *Angew*. *Chem*. *Int*. *Ed*. **2015**, *54*, 10639; b) Morimoto, Y.; Chen, F.; Matsuo, Y.; Kise, K.; Tanaka, T.; Osuka, A. Improved Synthesis of *ortho*-Phenylene-bridged Cyclic Tetrapyrroles and Oxidative Fusion Reactions Toward Substituted Tetraaza[8]circulenes. *Chem. Asian J.* **2021**, *16*, 648.

[17] Clar's sextet rule; Strutyński, K.; Mateo-Alonso, A.; Melle-Franco, M. Clar Rules the Electronic Properties of 2D π-Conjugated Frameworks: Mind the Gap. *Chem. Eur. J.* **2020**, *26*, 6569.

[18] Chen, F.; Tanaka, T.; Mori, T.; Osuka, A. Synthesis, Structures, and Optical Properties of Azahelicene Derivatives and Unexpected Formation of Azahepta[8]circulenes. *Chem. Eur. J.* **2018**, *24*, 7489.

[19] Matsuo, Y.; Tanaka, T.; Osuka, A. Highly Stable Radical Cations of N,N'-Diarylated Tetrabenzotetraaza[8]circulene. *Chem*. *Eur*. *J*. **2020**, *26*, 8144.

[20] Fuchter, M. J.; Weimar, M.; Yang, X.; Judge, D. K.; White, A. J. P. An unusual oxidative rearrangement of [7]-helicene, *Tetrahedron Lett.* **2012**, *53*, 1108.

[21] a) Schäfer, A.; Horn, H.; Ahlrichs, R. Fully optimized contracted Gaussian basis sets for atoms Li to Kr. *J. Chem. Phys.* **1992**, *97*, 2571; b) Weigend, F.; Ahlrichs, R. Balanced basis sets of split valence, triple zeta valence and quadruple zeta valence quality for H to Rn: Design and assessment of accuracy. *Phys. Chem. Chem. Phys.* **2005**, *7*, 3297.

[22] a) Grimme, S.; Antony, J.; Ehrlich, S.; Krieg, H. A consistent and accurate ab initio parametrization of density functional dispersion correction (DFT-D) for the 94 elements H-Pu. *J. Chem. Phys.* **2010**, *132*, 154104; b) Grimme, S.; Ehrlich, S.; Goerigk, L. Effect of the damping function in dispersion corrected density functional

theory. *J. Comput. Chem.* **2011**, *32*, 1456.

[23] Homodesmotic reaction; a) Minkin, V. I. Glossary of terms used in theoretical organic chemistry. *Pure Appl. Chem.* **1999**, *71*, 1919; b) George, P.; Trachtman, M.; Bock, C. W.; Brett, A. M. An alternative approach to the problem of assessing destabilization energies (strain energies) in cyclic hydrocarbons. *Tetrahedron* **1976**, *32*, 317.

[24] a) Johnson, E. R.; S. Keinan, S.; Mori-Sánchez, P.; Contreras-García, J.; Cohen, A. J.; Yang, W. Revealing Noncovalent Interactions. *J. Am. Chem. Soc.* **2010**, *132*, 6498; b) Contreras-García, J. Johnson, E. R.; Keinan, S.; Chaudret, R.; Piquemal, J.-P.; Beratan, D. N.; Yang, W. NCIPLOT: A Program for Plotting Noncovalent Interaction Regions. *J. Chem. Theory Comput.* **2011**, *7*, 625; c) Boto, R. A.; Peccati, F.; Laplaza, R.; Quan, C.; Carbone, A.; Piquemal, J.-P.; Maday, Y.; Contreras-García, J. NCIPLOT4: Fast, Robust, and Quantitative Analysis of Noncovalent Interactions. *J. Chem. Theory Comput.* **2020**, *16*, 4150.

[25] The HOMO-LUMO gap of **[n]AH'** is generally smaller than that of **[n]AH**, probably because of the effective conjugation along the helix.

[26] Shaidaei, H. F.-B.; Wannere, C. S.; Corminboeuf, C.; Puchta, R.; Schleyer, P. v. R. Which NICS Aromaticity Index for Planar π Rings Is Best? *Org. Lett.* **2006**, *8*, 863.

[27] Krygowski, T. M.; Szatylowicz, H.; Stasyuk, O. A.;. Dominikowska, J.; Palusiak, M. Aromaticity from the Viewpoint of Molecular Geometry: Application to Planar Systems. *Chem. Rev.* **2014**, *114*, 6383.

[28] a) Herges, R.; Geuenich, D. Delocalization of Electrons in Molecules. *J. Phys. Chem. A* **2001**, *105*, 3214; b) Geuenich, D.; Hess, K.; Köhler, F.; Herges, R. Anisotropy of the Induced Current Density (ACID), a General Method To Quantify and Visualize Electronic Delocalization. *Chem. Rev.* **2005**, *105*, 3758.

[29] a) Martin, R. E.; Diederich, F. Linear Monodisperse π-Conjugated Oligomers: Model Compounds for Polymers and More. *Angew. Chem. Int. Ed.* **1999**, *38*, 1350; b) Rieger, R.; Müllen, K. Forever young: polycyclic aromatichydrocarbons as model cases for structuraland optical studies. *J. Phys. Chem.* **2010**, *23*, 315.

[30] a) Chen, F.; Hong, Y. S.; Kim, D.; Tanaka, T.; Osuka, A. Sequential N-Alkylations of Tetrabenzotetraaza[8]circulene as a Tool To Tune Its Optical Properties. *ChemPlusChem* **2017**, *82*, 1048; b) Matsuo, Y.; Chen, F.; Kise, K.; Tanaka, T.; Osuka, A. Facile synthesis of fluorescent hetero[8]circulene analogues with tunable solubilities and optical properties. *Chem. Sci.* **2019**, *10*, 11006.

[31] In the case of **[13]AH, [15]AH**, and even longer, the corresponding C_s symmetric structure was found not to be the transition state probably due to the existence of multiple intermediacy structures. A similar trend is known for the racemization of [n]carbohelicenes which are estimated to have 2n-14 intermediates for n >7. Barroso, J.; Cabellos, J. L.; Pan, S.; Murillo, F.; Zarate, X.; Fernandez-Herrera, M. A.; Merino, G. *Chem. Commun.* **2018**, *54*, 188.